Northumbria Research Link

Citation: Ziyu Xing, Ziyu Xing, Haibao Lu, Haibao Lu, Sun, Ansu, Fu, Richard, Shahzad, Muhammad Wakil and Xu, Bin (2021) Understanding complex dynamics of interfacial reconstruction in polyampholyte hydrogels undergoing mechano-chemo-electrotaxis coupling. Journal of Physics D: Applied Physics, 54 (8). 085301. ISSN 0022-3727

Published by: IOP Publishing

URL: https://doi.org/10.1088/1361-6463/abc649 <https://doi.org/10.1088/1361-6463/abc649>

This version was downloaded from Northumbria Research Link: http://nrl.northumbria.ac.uk/id/eprint/44652/

Northumbria University has developed Northumbria Research Link (NRL) to enable users to access the University's research output. Copyright © and moral rights for items on NRL are retained by the individual author(s) and/or other copyright owners. Single copies of full items can be reproduced, displayed or performed, and given to third parties in any format or medium for personal research or study, educational, or not-for-profit purposes without prior permission or charge, provided the authors, title and full bibliographic details are given, as well as a hyperlink and/or URL to the original metadata page. The content must not be changed in any way. Full items must not be sold commercially in any format or medium without formal permission of the copyright holder. The full policy is available online: http://nrl.northumbria.ac.uk/policies.html

This document may differ from the final, published version of the research and has been made available online in accordance with publisher policies. To read and/or cite from the published version of the research, please visit the publisher's website (a subscription may be required.)

Northumbria University NEWCASTLE

University Library

Understanding complex dynamics of interfacial reconstruction in polyampholyte hydrogels undergoing mechano-chemo-electrotaxis coupling

Ziyu Xing[1], Haibao Lu[1,3], Ansu Sun[2], Yong Qing Fu[2], Muhammad Wakil Shahzad[2] and Ben Bin Xu[2,3]

[1]National Key Laboratory of Science and Technology on Advanced Composites in Special Environments, Harbin Institute of Technology, Harbin 150080, China

[2]Faculty of Engineering and Environment, Northumbria University, Newcastle upon Tyne, NE1 8ST, UK

[3]Corresponding author, E-mail: luhb@hit.edu.cn and ben.xu@northumbria.ac.uk

ABSTRACT: Polyampholyte (PA) hydrogels have attracted significant attentions for their superior mechanical strength and toughness compared with other conventional hydrogels. In this study, we present a novel thermodynamic approach to understand the mechano-chemo-electrotaxis coupling and interfacial dynamics in the PA hydrogels. Flory-Huggins theory, carried through an interfacial free-energy model, is the foundation for quantitative study of mechanically constitutive relationship of the PA gels. The proposed free-energy model is further extended to describe the mechano-chemo-electrotaxis switching and interfacial dynamics by co-relating Williams-Landel-Ferry equation and scaling laws. It was concluded that the interfacial bonding strength is the key factor to influence mechanical strength and reconstruction reversibility of the PA macromolecular gel system. The resulted analytical outcomes showed good agreement with the reported experimental data. We opine that the proposed model will guide the future application of PA hydrogels.

Keywords: polyampholyte hydrogel; interfacial dynamics; coupling model

1. Introduction

Hydrogel represents a group of important soft matters with versatile features, such as bespoken biocompatibility [1], superior biodegradability [2] and high stretchability [3]. The intrinsic nature of low macromolecular concentration in hydrogel usually results into a relatively low Young's modulus and a reasonable elasticity [4,5], to enable important potential for the applications in biological/biomedical engineering [1,2,6]. On the other hand, such low macromolecular concentration also limits the wide-range engineering applications of these materials due to environmental impact on the mechanical properties such as brittleness, un-scalability and non-adaptivity [7-12].

However, Polyampholyte (PA) hydrogel has been recently discovered with a potential to overcome its limitations and improve properties such as mechanical strength, elongation and tensile strength to 1-10MPa, 1000% and 100-1000J/m^2 respectively [13]. The molecular structure for PA hydrogels normally consists of the strong bonds working as permanent crosslinking points and the weak bonds working as reversible sacrificial [12,14]. Under mechanical loading, the weak bonds breaks first to dissipate the mechanical energy through a reversibly mechanochemical transition [15-20], while the strong bonds are served as permanent crosslinking points to dissipate the mechanical energy through deformation. Therefore, mechanical properties of PA hydrogels can be tuned by adjusting the interplays within and

between these two types of bonds, through ionic dissociation of polyelectrolyte [21-29].

Stimuli-responsive units can be introduced into PA hydrogel networks thus to create controlling mechanism which holds great potentials in designing soft robots, actuators, transducers and electronics [30-32]. For example, graphene oxide reinforced PA hydrogel was employed to improve the absorption capacities of Pb(II) and Cd(II) [33]. Cryoprotectant was introduced to enable the PA hydrogel to react with biological cell [34]. Similarly, PA hydrogel made from graft copolymers were used to achieve a high protein protection efficiency [35]. The PA hydrogel was investigated by many researchers. For example, Sun et al. reported an interesting PA hydrogel technology with high toughness and viscoelasticity, where the multi-field coupling was identified as a key parameter for the improved properties [36]. Khokhlov et al. used the transition theory to investigate the thermodynamic properties of the PA hydrogel and understand the dependence of the network dense state on the kosmotropic salt and specific ligands [37]. Relevant experimental studies conducted by Kudaibergenov showed that interfacial bonding strength of the PA hydrogel is greatly affected by ion species (K^+, Na^+, Mg^{2+}) and a significant swelling (about 500% decrease) was observed when PH value changed from 2 to 11 [38].

By far, most of literature focused on the optimization of PA hydrogel's mechanical properties by designing the molecular networks [8,12,18]. There is dearth of research on theoretical understandings towards the complicated interfacial interactions and conformational elasticity [22,24]. In our earlier work, strategies to understand the

structure-property relationships in the PA hydrogels, e.g. using a viscoelastic model [13] and a cooperative dynamics model [39] to describe their relaxation behaviours were explored. However, the interfacial interactions between two components with cationic and anionic groups, and their linking with mechanical properties of the PA hydrogel have not been investigated. In this work, a novel thermodynamic approach is introduced to understand the mechano-chemo-electrotaxis coupling and interfacial dynamics in the PA hydrogels, where the networks undergo a reversible reconstruction in response to an external mechanical loading. Based on the classical Flory-Huggins theory, we introduce interface interaction for the first time to simulate mechano-chemo-electrotaxis coupling effect in PA hydrogel, of which the constitutive stress-strain relation of PA hydrogel is originated from electrostatic short-range interaction instead of phenomenological mechanical model. Specifically, coupling effect and interfacial bonding strength of the PA hydrogels will be studied based on Williams-Landel-Ferry (WLF) [40] and scaling laws [41]. An interfacial free-energy model is developed and verified by comparing the obtained analytical results with the reported experimental data. We expect that this study will offer an effective insight on designing high performance PA hydrogels in terms of interfacial dynamics.

2. Theoretical framework

For the PA hydrogel, the polymer network mixed with water molecules is thermodynamically governed by Flory-Huggins theory [40], the free-energy equation at a temperature of T(K) can be written as,

$$\Delta F_M = RT(n_1 \ln \phi_1 + n_2 \ln \phi_2 + \chi n_1 \phi_2) \tag{1}$$

where ΔF_M is mixing free-energy, n_1 and ϕ_1 represent molar and volume fractions of solvent, respectively. n_2 and ϕ_2 represent molar and volume fractions of hydrogel, respectively. χ is the interactive parameter and R is the gas constant.

According to the Flory-Huggins theory, the interactive parameter (χ) is determined by temperature and weight fraction of water (ϕ_2) as,

$$\chi = \frac{A}{T} + B\phi_2 + C \tag{2}$$

where A, B and C are material constants.

Meanwhile, elastic free-energy (ΔF_{el}) of the PA hydrogel is governed by the rubber-elastic theory [40], e.g.,

$$\Delta F_{el} = \frac{3\xi k_B T}{2}[(\frac{1}{\phi_2})^{2/3} - 1] \tag{3}$$

where $k_B = 1.38\times10^{-23} J/K$ is Boltzmann constant, ξ refers to the number of monomer.

The free-energy function of the PA hydrogels should be the sum of the above two terms, e.g., $\Delta F = \Delta F_M + \Delta F_{el}$, while $\phi_1 = 1 - \phi_2 = \frac{V}{V+V_0}$, $V + V_0 = \lambda^3$ and $V_0 = \lambda_0^3$ [40]. From Equations (1) and (3), the free-energy function of PA hydrogel can be written as,

$$\Delta F = -RTn_1[\ln\frac{\lambda^3-\lambda_0^3}{\lambda^3} + \nu\frac{\lambda^3-\lambda_0^3}{\lambda_0^3}\ln\frac{\lambda_0^3}{\lambda^3} + (\frac{A}{T} + B\frac{\lambda_0^3}{\lambda^3} + C)\frac{\lambda_0^3}{\lambda^3}] + \frac{3\xi k_B T}{2}[\frac{\lambda^2}{\lambda_0^2} - 1] \tag{4}$$

where λ_0 is the pre-stretched elongation ratio, λ is the isotropic elongation ratio (where $\lambda = \lambda_1 = \lambda_2 = \lambda_3$), ν is the molar volume ratio of polymer monomer to water molecule [40]. Equations (1) to (4) are obtained from the Flory-Huggins theory and

rubber elasticity theory.

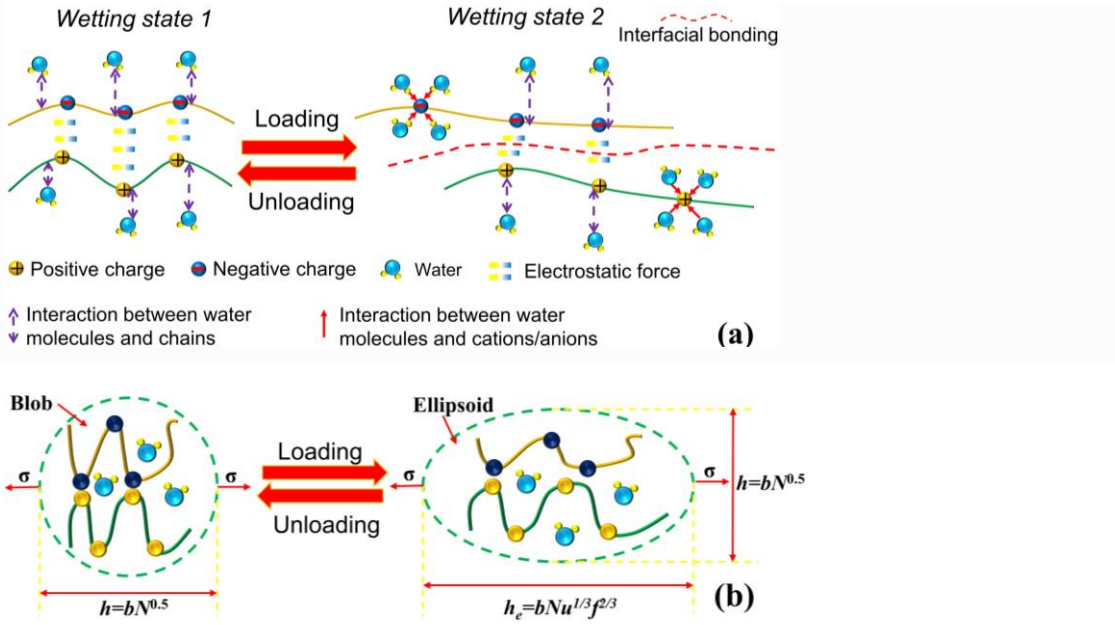

Fig. 1. (a) Illustrations of mechano-chemo-electrotaxis coupling and interfacial dynamics of PA network under the reversibly mechanical loading. **(b)** Illustrations of stress-induced deformation of PA network under the reversibly longitudinal stress.

As shown in **Fig. 1**, under a longitudinal stress (σ) applied to the hydrogels [40,41], the elastic free-energy (ΔF_{el}) is gradually increased according to the increased longitudinal stretching ratio (λ), whereas $\sigma=\frac{\partial \Delta F_{el}}{\partial \lambda}>0$. On the other hand, the mixing free-energy is changed due to the mechanochemical breaking of weak bonds into cationic and anionic end groups. However, these two groups attract each other owing to the existence of electrostatic forces, thus leading to complex mechano-chemo-electrotaxis interfacial interactions. Therefore, an interfacial free-energy is defined based on the mechano-chemo-electrotaxis coupling effect, as being illustrated in **Fig. 1(a)**. While the deformation of PA hydrogel network during the stretching process is anisotropic, the deformation from longitudinal direction

(same as the stretching direction) is different from that of the transverse direction (perpendicular to the stretching direction). Therefore, the PA network likely undergoes a stress-induced deformation in an ellipsoid shape [40], as shown in **Fig. 1(b)**. On the other hand, the cationic and anionic groups within PA hydrogel lead to different interfacial dynamic compared with other conventional hydrogels, lead to a high mechanical strength enabled by the mechano-chemo-electrotaxis interface coupling effect, caused by the electrostatic forces between cationic and anionic groups.

It is critical to understand the effect of interfacial interactions within the complex PA hydrogels system. According to an earlier studies [40], the interfacial energy function (ΔF_{int}) can be written as,

$$\Delta F_{\text{int}} = \gamma_{12}\Sigma = \pi k_B T \sqrt{\frac{\chi_{12}}{6}} N^{3/2} (\frac{l_B}{b})^{1/3} f^{2/3} \tag{5}$$

where $\gamma_{12} = \frac{k_B T}{b^2}\sqrt{\frac{\chi_{12}}{6}}$ is the interfacial tension, $\Sigma = \pi b^2 N^{3/2} (\frac{l_B}{b})^{1/3} f^{2/3}$ is the interfacial area, N is the number of polymer monomer, $b = 6nm$ is the length of polymer monomer [40], χ_{12} is the interactive parameter of two networks, f is the molar fraction of charge, $l_B = \frac{e^2}{\varepsilon_e k_B T}$ is the dielectric equilibrium length, ε_e is the dielectric constant, and $e = 1.6\times10^{-19} C$ is the charge quantity.

The constitutive relationship between the volume concentration and the polymer molecular weight can be scaled based on the reported correlation presented in [41],

$$C_{con} \propto M^{-\frac{4}{5}} \propto g^{-\frac{4}{5}} \propto l^{-8} \tag{6}$$

where C_{con} is the volume concentration of polymer monomer, M is the molecular

weight, g is the number of monomer and l is the monomer length. According to Equation (6), the number of monomer (N) can be scaled as:

$$N \propto \frac{g}{l} \propto M^{\frac{9}{10}} \propto C_{con}^{-\frac{9}{8}} \tag{7}$$

Combining Equations (3), (4), (6) and (7), the free-energy function of PA hydrogel can be expanded in the following equation:

$$\begin{aligned}\Delta F = \Delta F_{el} + \Delta F_M + \Delta F_{\text{int}} &= -RTn_1[\ln\frac{\lambda^3-\lambda_0^3}{\lambda^3} + \nu\frac{\lambda^3-\lambda_0^3}{\lambda_0^3}\ln\frac{\lambda_0^3}{\lambda^3} + (\frac{A}{T} + B\frac{\lambda_0^3}{\lambda^3} + C)\frac{\lambda_0^3}{\lambda^3}] \\ &+ \frac{3\xi k_B T}{2}[\frac{\lambda^2}{\lambda_0^2} - 1] + RTn_1\pi\sqrt{\frac{C_{\chi N}}{6}}k_N(\frac{l_B}{b})^{1/3} f_0^{2/3}\frac{\lambda^{\frac{11}{8}}}{\lambda_0^{\frac{11}{8}}}\end{aligned} \tag{8}$$

where k_N is a scaling constant and $f_0^{2/3}\sqrt{\frac{C_{\chi N}}{6}} \approx 1$ [41]. According to Equation (8), the constitutive stress-strain relationship can be written as:

$$\begin{aligned}\sigma = \frac{\partial \Delta F}{\partial \lambda} &= RTn_1\{[\frac{3(1-\nu)\lambda_0^3}{\lambda(\lambda^3-\lambda_0^3)} + 3\nu\frac{3\lambda^2\lambda_0^3}{(\lambda^3-\lambda_0^3)^2}\ln\frac{\lambda}{\lambda_0} - (\frac{3A}{T} + 6B\frac{\lambda_0^3}{\lambda^3} + 3C)\frac{\lambda_0^3}{\lambda^4}] \\ &+ \frac{3\xi}{N_A n_1}\frac{\lambda}{\lambda_0^2} + \frac{11\pi}{8}k_N(\frac{e^2}{\varepsilon_e k_B T b})^{1/3}\frac{\lambda^{\frac{3}{8}}}{\lambda_0^{\frac{11}{8}}}\} + L\end{aligned} \tag{9}$$

where L is remaining items of stress. RTn_1 is the modulus introduced by rubber elasticity theory [40,44], ν is the molar volume ratio of polymer monomer to water molecule, B is the coefficient of gel content (see equation (2)), $\frac{A}{T}+C$ is defined as coefficient between interaction parameters and temperature ($\frac{A}{T}+C$=0.5 for hydrogel [40,41]), λ_0 is the pre-stretched elongation ratio, $\frac{3\xi}{N_A n_1}$ is the ratio of elastic network density.

Based on the time-temperature equivalence principle [40,42], the constitutive relationship of relaxation time ($1/\omega$) and temperature (T) can be expressed as,

$$\sigma(T,\omega)=\sigma(T_0,a_T\omega) \tag{10}$$

where a_T is shift factor, and $\lg a_T=\frac{-17.44(T-T_g)}{51.6+(T-T_g)}$. By substituting Equation (10) into Equation (9), the effect of relaxation time on the constitutive stress-strain relationship can be generated.

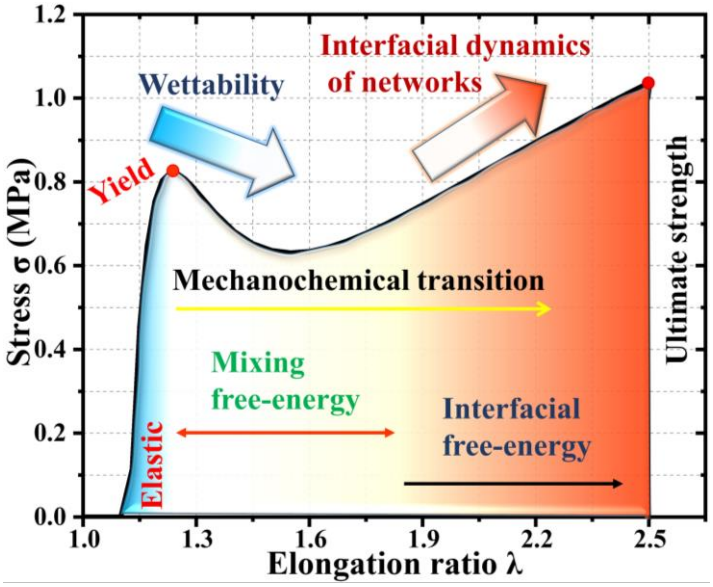

Fig. 2. Stress-elongation ratio graph of PA hydrogels with mechano-chemo-electrotaxis coupling and interfacial dynamics. Mechanochemical kinetics is determined by the mixing and interfacial free-energies.

Initially, PA hydrogel appears to be elastic and reversible following Hooke's law as shown in **Fig 2**. Once stress increase beyond the yield point, a permanent plastic deformation occurs. At this point, the stress-elongation ratio curve is dominated by the mixing and interfacial free-energies, rather than the elastic energy. Under a longitudinal loading, the strong bonds within PA hydrogel, which acts as permanent crosslinks, undergoes an elastic deformation, whilst the weak bonds work as reversible sacrificial bonds to dissipate the mechanical energy, through dissociating ironical couples in the PA gel. In particular, the electrostatic forces generated by the

cationic and anionic groups, change the interfacial equilibrium and alter the behaviour of hydrogel. The bonding strength in interface becomes significant under the strong bond confinement in an elastically responsive hydrogel [43].

Table 1. Values used in Equation (9) for the analytical calculations, where $\frac{A}{T}+C$ =0.5.

RTn_1	ν	B	λ_0	$\frac{3\xi}{N_A n_1}$	k_N	L
0.94	0.5	2	1	0.3	124	0

The analytical results using the proposed model are plotted in **Fig. 3**, with all input parameters listed in **Table 1**. **Fig. 3(a)** reveals that the maximum stress strength of hydrogel is increased from 0.631 MPa to 0.855 MPa at an elongation ratio of λ=1.23, with an increase in number of monomer (*N*) from 60 to 156. By increasing the number of monomers, the volume concentration of polymers in the hydrogel increases, thus yield a larger mechanical strength at the same elongation ratio. According to the rubber-elastic theory [40,44], the elastic modulus of polymer network is determined by the number of macromolecules per volume. A large number of macromolecules per single polymeric unit will result in a high elastic modulus and strength to resist the external mechanical loading. **Fig. 3(b)** shows the effect of dielectric constant (ε_e) on stress as a function of elongation ratio. It is found that the maximum stress strength decreases from 1.119 MPa to 0.742 MPa with an increase of ε_e from 1 to 5. With an increase in the dielectric constant of PA gel, a low interfacial bonding strength is obtained between the two components of cationic and anionic groups, thus resulting in a reduction in the stress strength of PA hydrogel.

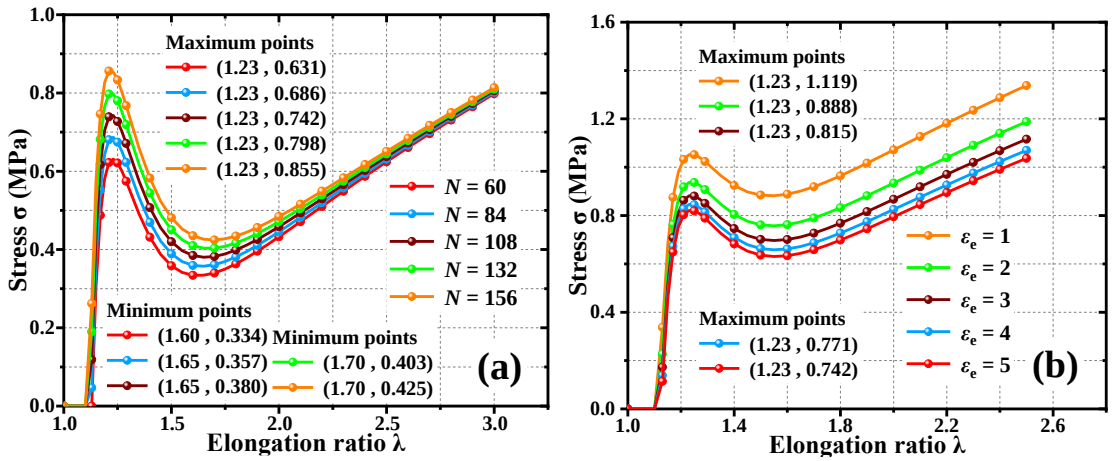

Fig. 3. Analytical results of stress as a function of elongation ratio for PA hydrogel. **(a)** At a monomer number of N=60, 84, 108, 132 and 156. **(b)** At a dielectric constant of ε_e =1, 2, 3, 4 and 5.

3. Experimental verification

3.1 Yielding behaviour of PA hydrogel

Three groups of experimental data of PA hydrogels (reported in Ref. [45]) have been collected to verify the analytical results generated from the proposed model, namely; (1) p-PA (p-PA is physical poly(NaSS-co-MPTC), where NaSS represents sodium *p*-styrenesulfonate and MPTC represents 3-(methacryloylamino)propyltrimethylammonium chloride); (2) c-PA1 (p-PA is chemically cross-linked with 0.01mol% gels); and (3) c-PA2 (p-PA is chemically cross-linked with 0.1mol% gels). Furthermore, the working principle and constitutive stress-strain relationship are obtained using these analytical and experimental results. The input values for p-PA, c-PA1 and c-PA2 hydrogels are listed in **Table 2**.

Based on the Equation (9), the nominal stresses as a function of tensile strain are plotted in **Fig. 4(a)**. It is found that the analytical results have good agreement with the experimental data that were previously reported in Ref. [45]. The yield stress was

calculated as σ =0.59 MPa, σ =0.92 MPa and σ =1.18 MPa for the p-PA, c-PA1 and c-PA2 hydrogels, respectively. It is found that the yielding strains of the hydrogels are decreased from ε =1.10, ε =0.64 to ε =0.21 with an increase in the yielding stress. The ultimate stress values are obtained as 2.81 MPa, 1.87 MPa and 1.59 MPa for the p-PA, c-PA1 and c-PA2 hydrogels, respectively. These analytical and experimental results reveal that the yielding strength of PA hydrogel can be significantly enhanced from 0.59 MPa to 1.18 MPa, with an increase in the molar content of cross-linker. However, the ultimate strength drops from 2.81 MPa to 1.59 MPa. Moreover, the divergences between the analytical and experimental results have been calculated based on correlation index (R^2), and the values are 97.55%, 87.40% and 94.90% for the p-PA, c-PA1 and c-PA2 hydrogels, respectively, as shown in **Fig. 4(b)**.

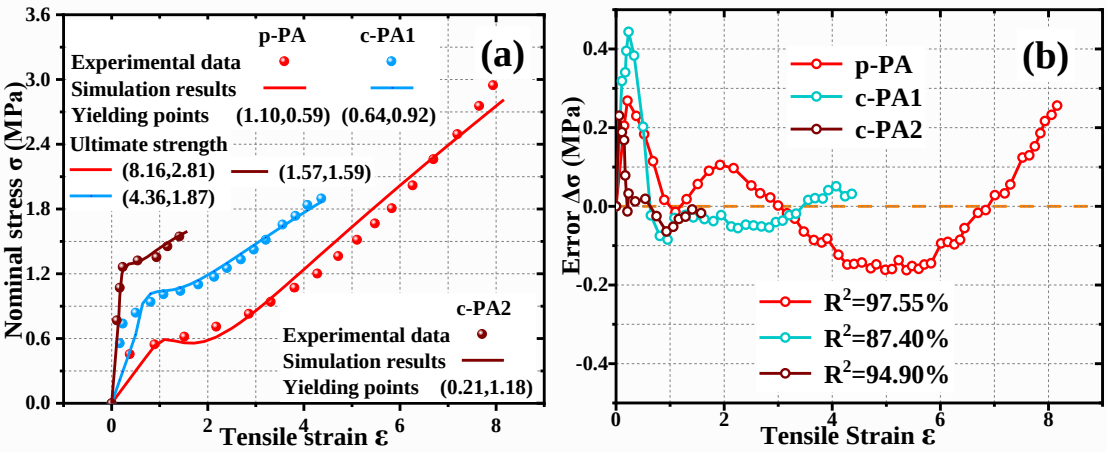

Fig. 4. Analytical results and experimental data [45] of tensile stress-strain curves and yielding strength of p-PA, c-PA1 and c-PA2 hydrogels. **(a)** For stress-strain curves. **(b)** Error ratio of nominal stress.

Table 2. Values used in Equation (9) for the p-PA, c-PA1 and c-PA2 hydrogels,

where $\frac{A}{T}+C$ =0.5 and ε_e =1.0.

	RTn_1	ν	B	λ_0	$\frac{3\xi}{N_A n_1}$	k_N	L
p-PA	1.47	0.4	1.9	4	0.88	56	-1.6
c-PA1	0.9	0.5	1.8	3	0.7	93	-0.1
c-PA2	0.65	0.55	1.7	1	0.12	124	0.95

We next use the experimental results of p-PA hydrogel (reported in Ref. [46]) to further verify the cyclically mechanical stress-strain behaviours predicted using our model. The inputs used in the calculation are listed in **Table 3**. Under the cyclically mechanical loading, the effects of stress and relaxation time on viscoelastic behaviours of p-PA hydrogel are considered. During the mechanical loading, a tensile stress is applied to the p-PA hydrogel with a maximum strain of 300%. Then the loading is removed and the p-PA hydrogel is left to regain its permanent shape.

Table 3. Values used in Equation (9) for the p-PA hydrogel with various relaxation times, where $\frac{A}{T}+C$ =0.5.

	RTn_1	ν	B	λ_0	$\frac{3\xi}{N_A n_1}$	k_N	L
First loading	0.12	0.6	1.5	1	0.4	198	0.16
0.25 min	0.088	0.5	1.1	2.1	0.9	43	0.04
1 min	0.09	0.55	1.1	1.75	0.8	117	0.04
5 min	0.095	0.55	1.05	1.25	0.75	124	0.07
30 min	0.1	0.5	1.1	1	0.65	173	0.11

Comparisons of analytical and experimental results in **Fig. 5(a)**, show that the proposed model is able to well predict the experimental results. By increasing the

relaxation time from 0.25 min to 30 min, the recovery ratio of stress jumps from 54.8% to 94.1%, and the recovery ratio of strain elevates from 55.9% to 92.9%. This is due to a reversibly mechanochemical transition in the p-PA hydrogel, of which the weak bond undergoes breakage and polymerization in response to the cyclically mechanical loading [46]. Therefore, the mechanical behaviour of p-PA hydrogel is essentially determined by both the relaxation time and mechanochemical kinetics, which lead to a significant enhancement of the mechanical stress from 0.289 MPa to 0.496 MPa when the relaxation time raises from 0.25 min to 30 min [46]. In **Fig. 5(b)**, the divergences between the analytical and experimental results of the p-PA hydrogel are also calculated using correlation index (R^2), and the results are 98.16%, 98.48%, 99.15%, 99.10% and 97.98% for first loading, 0.25 min, 1 min, 5 min and 30 min, respectively.

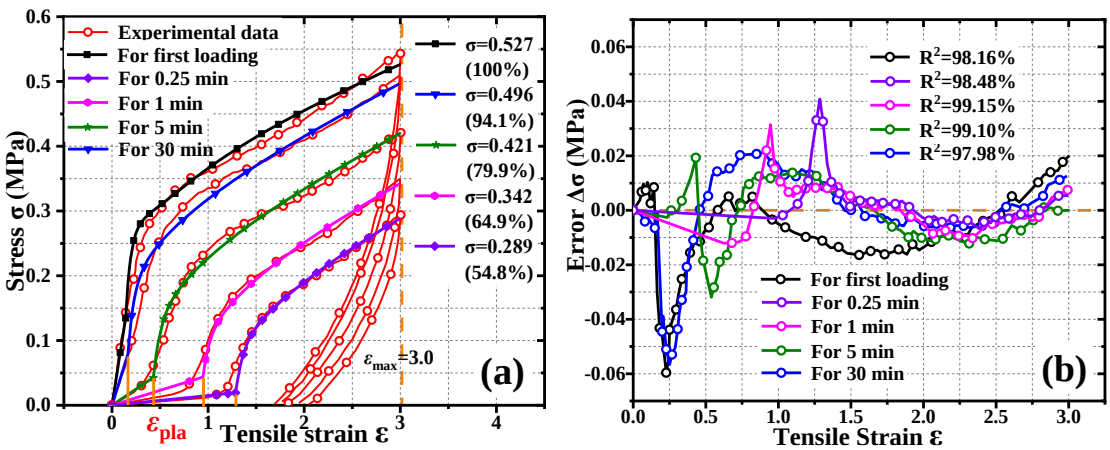

Fig. 5. Stress-strain curves and cyclically mechanical behaviour of p-PA hydrogel with various relaxation times of 0.25 min, 1 min, 5 min and 30 min, where $\frac{A}{T}+C$ =0.5. **(a)** For stress-strain curves. **(b)** Error ratio of stress.

3.2. Interfacial dynamics in PA hydrogel

As stated above, the mechanical behaviour of PA hydrogels is critically determined by their interfacial dynamics, where the interfacial bonding strength can be influenced by the dielectric constants of networks [36,46]. We also explored the effect of dielectric constant on mechanical behaviour of the PA hydrogel, e.g., poly(NaSS-co-DADMAC) (NaSS: sodium *p*-styrenesulfonate and PDADMAC: diallyldimethylammonium chloride). The inputs for the calculation are listed in **Table 4**.

Table 4. Values used in Equation (9) for PA hydrogels with various molar fractions of anion (f) and ionic monomer ($C_M(M)$), where $\frac{A}{T}+C=0.5$, f and $C_M(M)$ are given constants determined by the experiments [36,46].

f	RTn_1	ν	B	$\frac{3\xi}{N_A n_1}$	k_N	L
0.51	1.4	0.55	2	0.5	124	5.4
0.53	0.9	0.5	2	0.9	99	3.1
0.6	0.8	0.6	1.8	0.5	148	0.8
$C_M(M)$	RTn_1	ν	B	$\frac{3\xi}{N_A n_1}$	k_N	L
2.1	0.79	0.4	1.85	0.7	124	-0.66
2.0	0.65	0.4	1.85	0.67	130	-0.4
1.75	0.7	0.6	1.8	0.24	138	-0.03

Fig. 6(a) presented the stress-strain relationship of the PA hydrogels as function of the molar fraction of anion (f). It can be clearly seen that the experimental data with various molar fractions of anions have agreed well with the analytical results. The yielding stress is enhanced by more than 4.5 folds, from 1.60 MPa to 7.21 MPa, by

decreasing f from 0.60 to 0.51. The analytical results clearly show that the interfacial bonding strength is significantly improved when molar fraction of anion decreases, thus resulting in a plasticizing effect of water molecule on polymer networks and the increase of yielding stress [46].

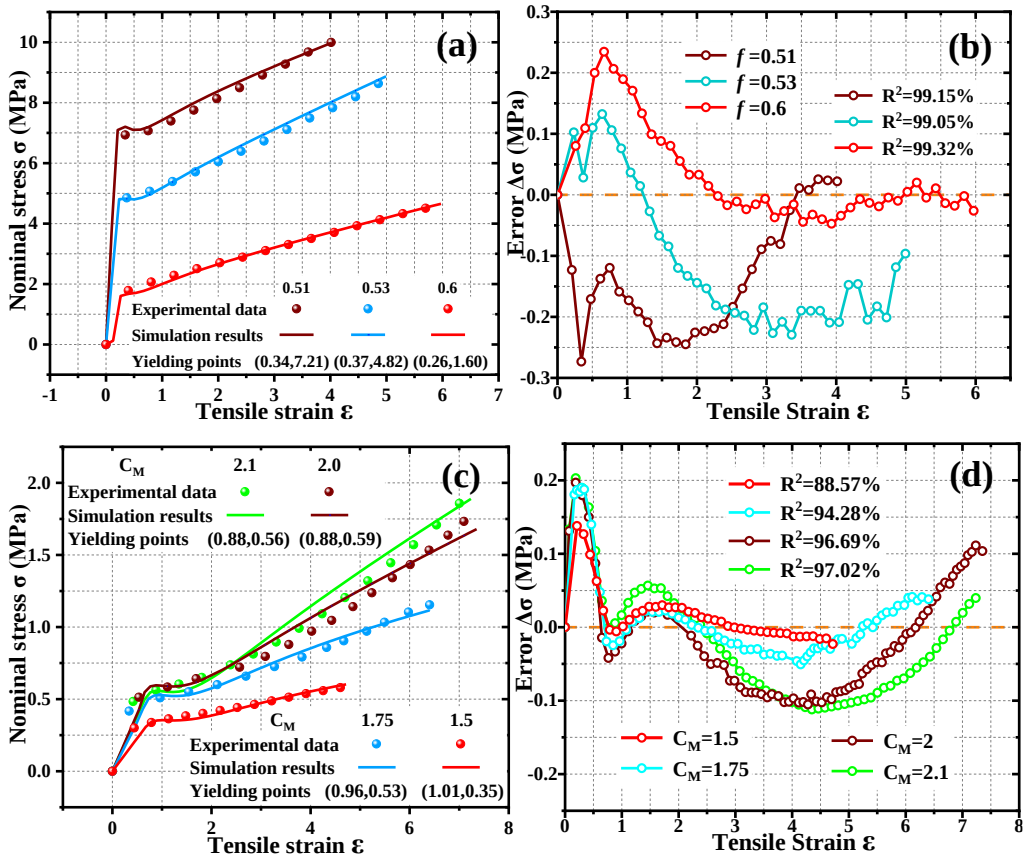

Fig. 6. **(a)** Analytical and experimental results [36,46] of nominal stress *versus* tensile strain at a given molar fraction of anion of f =0.51, 0.53 and 0.6. **(b)** Error ratio of nominal stress at a given molar fraction of anion. **(c)** Analytical and experimental results [36,46] of nominal stress *versus* tensile strain at a given molar concentration of ionic monomer of $C_M(M)$=2.1, 2.0, 1.75 and 1.5, where f =0.53, k_N =148 and L =1.7. **(d)** Error ratio of nominal stress at a given molar concentration of ionic monomer.

Fig. 6(b) shows the divergences between the analytical and experimental results

calculated by using correlation index (R^2). The data are 99.15%, 99.05% and 99.32% for a molar fraction of anion at 0.51, 0.53 and 0.6, respectively. We also investigate the effect of molar concentration of ionic monomer ($C_M(M)$) on the interfacial bonding strength for the PA hydrogel [36]. In **Fig. 6(c)**, it can be seen that the yield stress strength gradually increases from 0.35 MPa to 0.59 MPa when the molar concentration of ionic monomer increases from 1.5 to 2.0, due to a strong plasticizing effect of polymer networks that yield a large mechanical stress for the PA hydrogel. From above, the interfacial bonding strength between hydrotropic network and water has been proven as key player to determine the yielding stress in PA hydrogels. The divergences between the analytical and experimental results of PA hydrogels, calculated using correlation index (R^2) is shown in **Fig. 6(d)**, where a set of data of 88.57%, 94.28%, 96.69% and 97.02% are obtained with $C_M(M)$ of 2.1, 2.0, 1.75 and 1.5, respectively.

We further investigate the effect of relaxation time on mechanical behaviour of the PA hydrogel by using the inputs in **Table 5**, where parameters of $2\lambda_0 = \lambda - 1$, $T - T_g$ =10 K, $k_\omega = 2\times10^7 K\cdot s/m$ and $\omega = k_\omega i$ has been chosen for Equation (10). **Fig. 7(a)** shows the stress-strain curves of PA hydrogel with various deformation rates (i) of 900 mm/min, 400 mm/min and 70 mm/min. The reported experimental results in Ref. [36] are used to compare with the analytical data calculated from our model. The analytical results show that the yielding stress of PA hydrogels is increased from 0.46 MPa to 1.01 MPa, when the deformation rate is increased from 70 mm/min to 900 mm/min. Under a higher deformation rate, a vast amount of PA components is

involved in the mechanochemical transition, thus resulting in an increment in the interfacial free-energy [40,44] and a significant enhancement in yielding stress. In **Fig. 7(b)**, the divergences between the analytical and experimental results are obtained by calculating the correlation index (R^2), which are 97.31%, 98.15% and 98.15% at 70 mm/min, 400 mm/min and 900 mm/min, respectively.

Table 5. Values used in Equation (9) for PA hydrogel with various deformation rates (i), where $\frac{A}{T}+C$ =0.5.

i (mm/min)	Rn_1	ν	B	λ_0	$\frac{3\xi}{N_A n_1}$	k_N	L
900	2.6×10^{-3}	0.5	2	1	0.8	124	-0.4
400	4.5×10^{-3}				0.85		
70	1.4×10^{-2}				1		

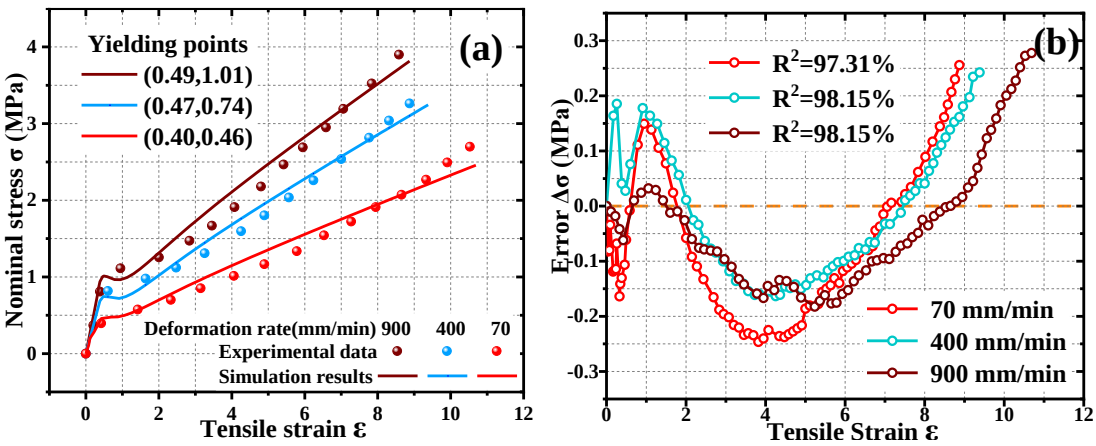

Fig. 7. **(a)** Analytical prediction curves and experimental data [36] of nominal stress as a function of tensile strain for PA hydrogels with various deformation rates. **(b)** Error ratio of nominal stress at a given deformation rate.

3.3. Fracture strength of PA hydrogel

The fracture strength of PA hydrogels, an important mechanical feature, is also determined by the mechano-chemo-electrotaxis coupling effect induced interfacial dynamics. We then evaluate the effect of interfacial dynamics on fracture strength. As previously introduced, the stress-induced deformation of PA network appears to be in an ellipsoid form under the longitudinal stress. Therefore, the cross-section area can be calculated as $\frac{(bN^{0.5})^2}{4}$ and interfacial force can be written as [40,44],

$$\frac{\partial \Delta F_{\text{int}}}{\partial \lambda_{\text{int}}} = \frac{\partial \gamma \pi \frac{(bN^{0.5})^2}{4}}{\partial \lambda} \tag{11}$$

where ΔF_{int} is the interface energy and γ is the interfacial tension.

According to Equations (2), (5), (6), (7) and (11), the elongation ratio follows,

$$\lambda_{\text{int}}\left(C_W\right) = [\frac{44}{27\gamma} l_B^{1/3} b^{-7/3}]^{8/19} (1 - C_W)^{-3/19} \tag{12}$$

Based on the Equation (12), the fracture strain (ε_b) can be expressed as,

$$\varepsilon_b\left(C_W\right) = [\frac{44}{27\gamma} l_B^{1/3} b^{-7/3}]^{8/19} (1 - C_W)^{-3/19} - \lambda_m \tag{13}$$

where C_W is water content and λ_m =47.05 is the given constant [40,44]. By combining Equations (11) and (13), the fracture stress is therefore presented as,

$$\begin{aligned} \sigma_b &= \frac{N_1^0}{\lambda^3} \frac{\partial \Delta F_{\text{int}}}{\partial \varepsilon_b} |_{\lambda = 1 + \varepsilon_b} \\ &= \frac{27 N_1^0 \gamma \pi k_N b^2}{32} \{1 + [\frac{44}{27\gamma} l_B^{1/3} b^{-7/3}]^{8/19} (1 - C_W)^{-3/19} - \lambda_m\}^{-\frac{5}{8}} \end{aligned} \tag{14}$$

where it is hypothesised that $[\frac{44}{27\gamma} l_B^{1/3} b^{-7/3}]^{8/19}$ =46 and $\frac{27 N_1^0 \gamma \pi k_N b^2}{32}$ =2.5 in Equations (13) and (14) for calculation. Equations (11), (12), (13) and (14) are derived from the equation (8).

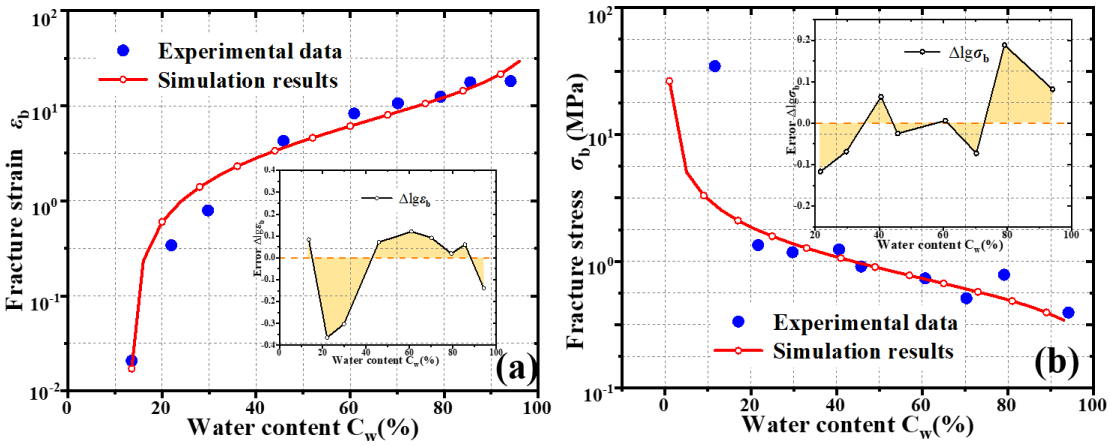

Fig. 8. Analytical results and experimental data [47] of fracture strength as a function of water content (C_W) in PA hydrogels. **(a)** For fracture strain. **(b)** For fracture stress.

Two groups of experimental data reported in Ref. [47] of the PDGI/PAAm PA hydrogels (PDGI, poly(dodecyl glyceryl itaconate); PAAm: poly(acrylamide)) have been employed to compare with our analytical results. The effects of water content on fracture strain and fracture stress are investigated. The plot of fracture strain and stress as a function of water content in PA hydrogel is presented in **Figs. 8(a)** and **8(b)**, respectively. It is found that the simulation results from our models are in good agreements with the experimental data of PA hydrogels. The mechano-chemo-electrotaxis coupling effect clearly affect the fracture strength, where the interfacial bonding strength between PA network and water molecules has been significantly improved due to the externally mechanical loading and the electrostatic forces of cationic and anionic groups. Under the event of large amount of cationic and anionic groups suddenly emerges due to the breaking of weak bonds, yield high statistical probability to create a strong interfacial bonding strength and hence significant improvement of fracture strength.

5. Conclusions

In this study, a thermodynamic approach is introduced to understand the unique mechano-chemo-electrotaxis coupling and interfacial dynamics in the PA hydrogels for the first time. Flory-Huggins theory is applied as the core analytical approach to formulate a constitutive framework to describe the complicated coupling and interfacial dynamics induced mechanical behaviour for PA hydrogel. By considering the monomer number, dielectric constant, relaxation time, molar fraction of anion, molar concentration of ionic monomer and deformation rate, an interfacial free-energy model is established to quantitatively understand the mechanical behaviour beyond the yield limit of for PA hydrogel. Reasonable agreements have been reached in most scenarios when comparing the analytical result with the previous reported experimental data. Moreover, the proposed model has been extended to explore the working principles of the mechano-chemo-electrotaxis coupling effect and interfacial dynamics, where the analytical data show a good fit to the experimental results. This novel model is expected to guide future design and development of PA hydrogels, with potential application in frontier engineering sectors.

Acknowledgements

This work was financially supported by the National Natural Science Foundation of China (NSFC) under Grant No. 11672342 and 11725208.

References

[1] Nonoyama T, Wada S, Kiyama R, Kitamura N, Mredha M I, Zhang X, Kurokawa T, Nakajima T, Takagi Y, Yasuda K and Gong J P 2016 Double-network hydrogels strongly bondable to bones by spontaneous osteogenesis penetration *Adv. Mater.* **28** 6740-5

[2] Zhao Y, Nakajima T, Yang J J, Kurokawa T, Liu J, Lu J, Mizumoto S, Sugahara K, Kitamura N, Yasuda K, Daniels A U D and Gong J P 2014 Proteoglycans and glycosaminoglycans improve toughness of biocompatible double network hydrogels *Adv. Mater.* **26** 436-42

[3] Hu Y, Du Z S, Deng X L, Wang T, Yang Z H, Zhou W Y and Wang C Y 2016 Dual physically cross-linked hydrogels with high stretchability, toughness, and good self-recoverability *Macromolecules* **49** 5660-8

[4] Dai X Y, Zhang Y Y, Gao L N, Bai T, Wang W, Cui Y L and Liu W G 2015 A mechanically strong, highly stable, thermoplastic, and self-healable supramolecular polymer hydrogel *Adv. Mater.* **27** 3566-71

[5] Yuk H W, Zhang T, Lin S T, Parada G A and Zhao X H 2016 Tough bonding of hydrogels to diverse non-porous surfaces *Nat. Mater.* **15** 190-6

[6] Kwon H J, Yasuda K, Ohmiya Y, Honma K, Chen Y M and Gong J P 2010 In vitro differentiation of chondrogenic ATDC5 cells is enhanced by culturing on synthetic hydrogels with various charge densities *Acta Biomater.* **6** 494-501

[7] Chen Q, Chen H, Zhu L and Zheng J 2016 Engineering of tough double network hydrogels *Macromol. Chem. Phys.* **217** 1022-36

[8] Gong J P 2010 Why are double network hydrogels so tough? *Soft Matter* **6** 2583-90

[9] Liu Y and Lee B P 2016 Recovery property of double-network hydrogel containing mussel-inspired adhesive moiety and nano-silicate *J. Mater. Chem. B.* **4** 6534-40

[10] Feng X, Ma Z, MacArthur J V, Giuffre C J, Bastawros A F and Hong W 2016 Highly stretchable double-network composite *Soft Matter* **12** 8999-9006

[11] Dai L, Tian C and Xiao R 2020 Modeling the thermo-mechanical behavior and constrained recovery performance of cold-programmed amorphous shape-memory polymers *Int. J. Plasticity* **127** 102654

[12] Gong J P, Katsuyama Y, Kurokawa T and Osada Y 2003 Double network hydrogels with extremely high mechanical strength *Adv. Mater.* **15** 1155-8

[13] Matsuda T, Nakajima T and Gong J P 2019 Fabrication of tough and stretchable hybrid double-network elastomers using ionic dissociation of polyelectrolyte in nonaqueous media *Chem. Mater.* **31** 3766-76

[14] Lu H B, Xing Z Y, Hossain M and Fu Y Q 2019 Modeling strategy for dynamic-modal mechanophore in double-network hydrogel composites with self-growing and tailorable mechanical strength *Compos. Part B-Eng.* **179** 107528

[15] Dopieralski P, Ribas-Arino J, Anjukandi P, Krupicka M and Marx D 2017 Unexpected mechanochemical complexity in the mechanistic scenarios of disulfide bond reduction in alkaline solution *Nat. Chem.* **9** 164-70

[16] Ducrot E, Chen Y, Bulters M, Sijbesma R P and Creton C 2014 Toughening elastomers with sacrificial bonds and watching them break *Science* **344** 186-9

[17] Diesendruck C E, Peterson G I, Kulik H J, Kaitz J A, Mar B D, May P A, White S R, Martínez T J, Boydston A J and Moore J S 2014 Mechanically triggered heterolytic unzipping of a low-ceiling-temperature polymer *Nat. Chem.* **6** 623-8

[18] Nakajima T, Takedomi N, Kurokawa T, Furukawa H and Gong J P 2010 A facile method for synthesizing free-shaped and tough double network hydrogels using physically crosslinked poly(vinyl alcohol) as an internal mold *Polym. Chem.* **1** 693-7

[19] Ahmed S, Nakajima T and Kurokawa K 2014 Brittle-ductile transition of double network hydrogels: Mechanical balance of two networks as the key factor *Polymer* **55** 914-23

[20] Sun T L, Luo F, Hong W, Cui K P, Huang Y W, Zhang H J, King D R, Kurokawa T, Nakajima T and Gong J P 2017 Bulk energy dissipation mechanism for the fracture of tough and self-healing hydrogels *Macromolecules* **50** 2923-31

[21] Koetting M C and Peters J T 2015 A comprehensive review of $Li_4Ti_5O_{12}$-based electrodes for lithium-ion batteries: The latest advancements and future perspectives *Mat. Sci. Eng. R* **93** 1-71

[22] Hong W, Zhao X H and Suo Z G 2010 Large deformation and electrochemistry of polyelectrolyte gels *J. Mech. Phys. Solids* **58** 558-77

[23] Marcombe R, Cai S Q, Hong W, Zhao X H, Laputsta Y and Suo Z G 2010 A theory of constrained swelling of a pH-sensitive hydrogel *Soft Matter* **6** 784-93

[24] Li J Y, Suo Z G and Vlassak J J 2014 A model of ideal elastomeric gels for polyelectrolyte gels *Soft Matter* **10** 2582-90

[25] Zhang H J, Sun T L, Zhang A K, Nakajima T, Nonoyama T, Kurokawa T, Ito O, Ishitobi H and Gong J P 2016 Tough physical double-network hydrogels based on amphiphilic triblock copolymers *Adv. Mater.* **28** 4884-90

[26] Na Y H, Tanaka Y, Kawauchi Y, Furukawa H, Sumiyoshi T and Gong J P 2016 Necking phenomenon of double-network gels *Macromolecules* **39** 4641-5

[27] Nakajima T, Kurokawa T, Ahmed S, Wu W L and Gong J P 2013 Characterization of internal fracture process of double network hydrogels under uniaxial elongation *Soft Matter* **9** 1955-66

[28] Zheng W J, Liu Z Q, Xu F, Gao J, Chen Y M, Gong J P and Osada Y 2015 In vitro platelet adhesion of PNaAMPS/PAAm and PNaAMPS/PDMAAm double-network hydrogels *Macromol. Chem. Phys.* **216** 641-9

[29] Matsuda T, Nakajima T, Fukuda Y, Hong W, Sakai T, Kurokawa T, Chung U I and Gong J P 2016 Yielding criteria of double network hydrogels *Macromolecules* **49** 1865-72

[30] Yang C, Liu Z, Chen C, Shi K, Zhang L, Ju X J, Wang W, Xie R and Chu L Y 2017 Reduced graphene oxide-containing smart hydrogels with excellent electro-response and mechanical properties for soft actuators *ACS Appl. Mater. Inter.* **9** 15758-67

[31] Fuhrer R, Athanassiou E K, Luechinger N A and Stark W J 2009 Crosslinking metal nanoparticles into the polymer backbone of hydrogels enables preparation of soft, magnetic field-driven actuators with muscle-like flexibility *Small* **5** 383-8

[32] Zheng W J, An N, Yang J H, Zhou J X and Chen Y M 2015 Tough Al-alginate/poly(N-isopropylacrylamide) hydrogel with tunable LCST for soft robotics *ACS Appl. Mater. Inter.* **7** 1758-64

[33] Zhou G, Luo J, Liu C, Chu L, Ma J, Tang Y, Zeng Z and Luo S 2016 A highly efficient polyampholyte hydrogel sorbent based fixed-bed process for heavy metal removal in actual industrial effluent *Water Res.* **89** 151-60

[34] Stubbs C, Bailey T L, Murray K and Gibson M I 2020 Polyampholytes as Emerging Macromolecular Cryoprotectants *Biomacromolecules* **21** 7-17

[35] Zhao D, Rajan R and Matsumura K 2019 Dual Thermo- and pH-Responsive Behavior of Double Zwitterionic Graft Copolymers for Suppression of Protein Aggregation and Protein Release *ACS Appl. Mater. Interfaces* **11** 39459-69

[36] Sun T L, Kurokawa T, Kuroda S, Ihsan A B, Akasaki T, Sato K, Haque M A, Nakajima T and Gong J P 2013 Physical hydrogels composed of polyampholytes demonstrate high toughness and viscoelasticity *Nat. Mater.* **12** 932-7

[37] Grinberga V Y, Burovaa T V, Grinberga N V, Alvarez-Lorenzob C and Khokhlov A R 2019 Protein-like energetics of conformational transitions in a polyampholyte hydrogel *Polymer* **179** 121617

[38] Kudaibergenov S E 2019 Physicochemical, complexation and catalytic properties of polyampholyte cryogels *Gels* **5** 1-22

[39] Xing Z Y, Lu H B, Hossain M, Fu Y Q, Leng J S and Du S Y 2020 Cooperative dynamics of heuristic swelling and inhibitive micellization in double-network hydrogels by ionic dissociation of polyelectrolyte *Polymer* **186** 122039

[40] Flory P J 1953 Principles of polymer chemistry. New York: Cornell University Press

[41] Gennes P G 1979 Scaling concepts in polymer physics. Ithaca and London :Cornell University Press

[42] Williams M L, Landell R F and Ferry J D 1995 The temperature dependence of relaxation mechanisms in amorphous polymers and other glass-forming liquids *J. Am. Chem. Soc.* **77** 3701-7

[43] Shin J, Cherstvy A G and Metzler R 2014 Sensing viruses by mechanical tension of DNA in responsive hydrogels *Phys. Rev. X* **4** 021002

[44] Treloar L R G 1975 The physics of rubber elasticity. New York: Oxford University

[45] Karobi S N, Sun T L, Kurokawa T, Luo F, Nakajima T, Nonoyama T and Gong J P 2016 Creep behavior and delayed fracture of tough polyampholyte hydrogels by tensile test *Macromolecules* **49** 5630-6

[46] Murakawa K, King D R, Sun T L, Guo H, Kurokaw T and Gong J P 2019 Polyelectrolyte complexation via viscoelastic phase separation results in tough and self-recovering porous hydrogels *J. Mater. Chem. B.* **7** 5296-305

[47] Ilyas M, Haque Md A, Yue Y F, Kurokawa T, Nakajima T, Nonoyama T and Gong J P 2017 Water-triggered ductile-brittle transition of anisotropic lamellar

hydrogels and effect of confinement on polymer dynamics *Macromolecules* **50** 8169-77

Tables caption

Table 1. Values used in Equation (9) for the analytical calculations, where $\frac{A}{T}+C$ =0.5.

Table 2. Values used in Equation (9) for the p-PA, c-PA1 and c-PA2 hydrogels, where $\frac{A}{T}+C$ =0.5 and ε_e =1.0.

Table 3. Values used in Equation (9) for the p-PA hydrogel with various relaxation times, where $\frac{A}{T}+C$ =0.5.

Table 4. Values used in Equation (9) for PA hydrogels with various molar fractions of anion (f) and ionic monomer ($C_M(M)$), where $\frac{A}{T}+C$ =0.5, f and $C_M(M)$ are given constants determined by the experiments [36,46].

Table 5. Values used in Equation (9) for PA hydrogel with various deformation rates (i), where $\frac{A}{T}+C$ =0.5.

Figures caption

Fig. 1. (a) Illustrations of mechano-chemo-electrotaxis coupling and interfacial dynamics of PA network under the reversibly mechanical loading. **(b)** Illustrations of stress-induced deformation of PA network under the reversibly longitudinal stress.

Fig. 2. Stress-elongation ratio graph of PA hydrogels with mechano-chemo-electrotaxis coupling and interfacial dynamics. Mechanochemical kinetics is determined by the mixing and interfacial free-energies.

Fig. 3. Analytical results of stress as a function of elongation ratio for PA hydrogel. **(a)** At a monomer number of N=60, 84, 108, 132 and 156. **(b)** At a dielectric constant of ε_e=1, 2, 3, 4 and 5.

Fig. 4. Analytical results and experimental data [45] of tensile stress-strain curves and yielding strength of p-PA, c-PA1 and c-PA2 hydrogels. **(a)** For stress-strain curves. **(b)** Error ratio of nominal stress.

Fig. 5. Stress-strain curves and cyclically mechanical behaviour of p-PA hydrogel with various relaxation times of 0.25 min, 1 min, 5 min and 30 min, where $\frac{A}{T}+C$ =0.5. **(a)** For stress-strain curves. **(b)** Error ratio of stress.

Fig. 6. **(a)** Analytical and experimental results [36,46] of nominal stress *versus* tensile strain at a given molar fraction of anion of f =0.51, 0.53 and 0.6. **(b)** Error ratio of nominal stress at a given molar fraction of anion. **(c)** Analytical and experimental results [36,46] of nominal stress *versus* tensile strain at a given molar concentration of ionic monomer of $C_M(M)$=2.1, 2.0, 1.75 and 1.5, where f =0.53, k_N=148 and L =1.7. **(d)** Error ratio of nominal stress at a given molar concentration of ionic

monomer.

Fig. 7. **(a)** Analytical prediction curves and experimental data [36] of nominal stress as a function of tensile strain for PA hydrogels with various deformation rates. **(b)** Error ratio of nominal stress at a given deformation rate.

Fig. 8. Analytical results and experimental data [47] of fracture strength as a function of water content (C_W) in PA hydrogels. **(a)** For fracture strain. **(b)** For fracture stress.